Characterisation of RF Connectors and Components for Advanced 5G Applications

Kimmo Rasilainen[1], Marko E. Leinonen[1], Olli Kursu[1], Klaus Nevala[1], Shayan Hasan Naushahi[1],
Juha-Matti Ojakoski[1], Markus Berg[1,2], and Aarno Pärssinen[1]
[1]Centre for Wireless Communications, University of Oulu, Finland
[2]ExcellAnt Oy, Oulu, Finland
e-mail: kimmo.rasilainen@oulu.fi

***Abstract*—Development of 5G and beyond technologies brings wireless communications systems to operate at higher frequencies and makes them more compact and integrated in nature. This places further challenges for component and system design, but at the same time the need for reliable RF interconnections becomes more and more important. This work investigates passive RF structures implemented on a low-permittivity Panasonic dielectric substrate up to a frequency of 110 GHz with simulations and measurements. Two different test cases are considered: a simple transmission line with a TRL calibration structure as well as a Wilkinson power divider. Agreement between simulations and measurements is rather good, and the results show that the used substrate material is a viable alternative for RF applications around 100 GHz.**

***Keywords*-connector, dielectric substrate, millimetre wave, transmission line, Wilkinson power divider, 5G.**

I. Introduction

We are currently witnessing a widespread commercial deployment of fifth generation (5G) communications networks and systems. From a technology point of view, this development is aiming to deliver, among some of the key metrics, higher data rates, bandwidths, and larger numbers of simultaneous users [1]. Frequency bands below 6 GHz have traditionally been used for wireless communications, but these are facing spectral congestion due to the existing networks and services. This, combined with a greater need for broader bandwidths is driving the research and design interests towards millimetre-wave frequencies (approximately 30 GHz and beyond).

At the same time, planning and early development of beyond-5G technologies (referred to as 6G), to be launched around 2030, are already ongoing (see, e.g., [2]–[4]). Compared to 5G, the requirements for 6G systems can roughly be estimated to have more than a tenfold improvement in many of the key performance metrics. Achieving envisioned data rates in the range of 1 Tbit/s requires the use of sub-THz/THz frequencies (e.g., around 300 GHz). However, such a generation shift in technology does not occur overnight, and it is foreseeable that the current technology will experience several enhancements and modifications when moving from 5G to 6G, including an "intermediate" phase that can be called Advanced 5G. An example of such intermediate stages is the so-called D-band at 110–170 GHz, which has recently gained significant interest as a solution for Beyond-5G technologies [5]–[7].

The aforementioned requirements pose new scientific and technical challenges for designers and engineers both on the network and hardware sides. As a result, key aspects in radio engineering include defining optimal RF architectures and selecting semiconductor technologies to obtain the required performance. Integration of the advanced, high-performance electronics to enable compact device sizes suitable for practical applications and finding appropriate materials and processes to achieve this are also of significant importance. Additionally, well-performing and reliable transmission lines and other interconnects are essential for signal routing and component connections.

When considering transmission lines (such as microstrip lines or coplanar waveguides), routing of the RF components and devices especially in integrated, multi-layer printed circuit boards (PCBs) requires careful consideration, e.g., by minimising their lengths to reduce the losses and matching of interconnection widths to reduce reflections. Despite this, the optimal PCB materials should be sufficiently low-loss (per unit length) to begin with. Therefore, the development of such materials and structures is an important research topic in monolithic integrated circuits as well as in integrated RF components and modules [8]–[10].

In this work, we address the material and interconnect issues by analysing the performance of passive transmission-line based test structures and components at millimetre-wave frequencies. Two different types of test structures and RF connectors are used, and their performance is investigated using both simulations and measurements.

II. Research Methodology and Test Structures

As a starting point, the structures have been designed using full-wave computer simulations. Electromagnetic simulations on the test structures have been carried out in CST Microwave Studio. Then, test structures have been manufactured based on the simulation models, and measurements have been performed using a vector network analyser and frequency extenders.

(a)

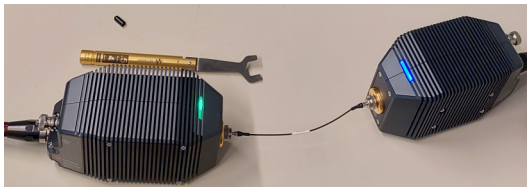

(b)

Figure 1. Photograph of the measurement setup: (a) PNA and mm-wave test set, and (b) two mm-wave extender modules connected back-to-back using a 1-mm coaxial cable.

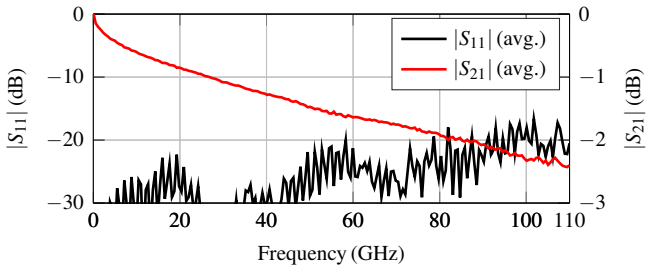

Figure 2. Average matching and insertion loss of 1-mm connector cables measured across four individual samples with two measurements each.

A. Methodology and Instrumentation Used

A Keysight N5242B PNA together with a Keysight N5292A PNA Millimetre Test Set are used to perform cable measurements up to a frequency of 110 GHz. The test set features frequency extenders with 1-mm coaxial connectors, and these can be used for coaxial measurements across a continuous frequency range from 10 MHz up to 110 GHz. Currently, this is the highest frequency and connector pair that has been specified in IEEE standards [11]. The chosen approach and frequency range enable an analysis of the performance and characteristics of the used structures from an Advanced 5G point of view.

Figure 1 shows a photograph of the used measurement hardware. This equipment is used together with the test structures through Rosenberger 01K80A-40ML5 1-mm SMD connectors, which are solderless and mounted onto the PCB with screws and guide pins [12]. The extenders and test

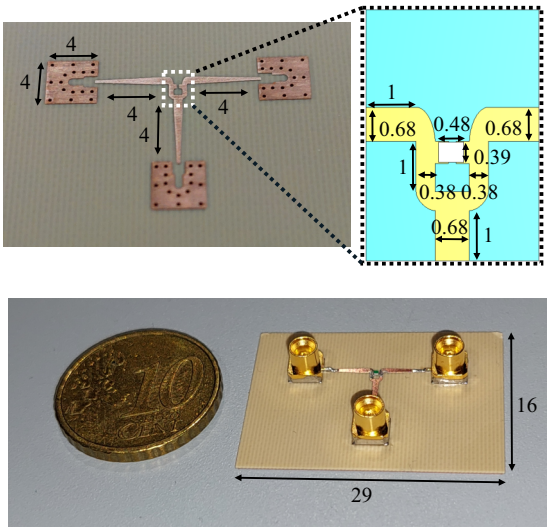

Figure 3. Photograph and CAD model of the test structure for the millimetre-wave Wilkinson power divider. Dimensions are in mm.

structures are connected using 1-mm coaxial cables, whose average measured S-parameters are displayed in Figure 2. The measurements have been performed for four individual cables, each of which have been measured twice. The length of the cables is 16 cm, which results in a maximum cable loss of 0.15 dB/cm at the studied frequencies.

The test structures are implemented on PCBs that utilise a Panasonic low Dk / low Df material as the substrate ($\varepsilon_\mathrm{r} = 3.34$, $\tan\delta = 0.004$ at 50 GHz) [13]. This substrate material is commonly used at lower frequencies up to the millimetre-wave range, and this work investigates its suitability for applications at frequencies up to around 100 GHz. This is one of the highest frequencies reported for this substrate; however studies for a similar/comparable material have been reported up to 160 GHz in [14], [15].

B. Wilkinson Power Divider

The first test structure is a symmetric Wilkinson power divider with an equal power division ratio between the two output ports. Illustration of the structure is given in Figure 3. This represents a well-known component in RF and microwave applications, and the design can also be generalised to N ports [16]. Example Wilkinson implementations for millimetre-wave frequencies can be found in, e.g., [17], [18]. The power dividers of this study have been implemented on a dual-layer PCB of the previous Panasonic dielectric material, with a substrate thickness of 300 µm and an 18-µm copper layer on either side of the dielectric. In the design, bends in the Wilkinson power divider structure were rounded to avoid additional reactive effects caused by sharp corners. The power dividers use Mini-SMP (SMPM) connectors which operate up to a frequency of 65 GHz.

According to the basic topology, the output branches

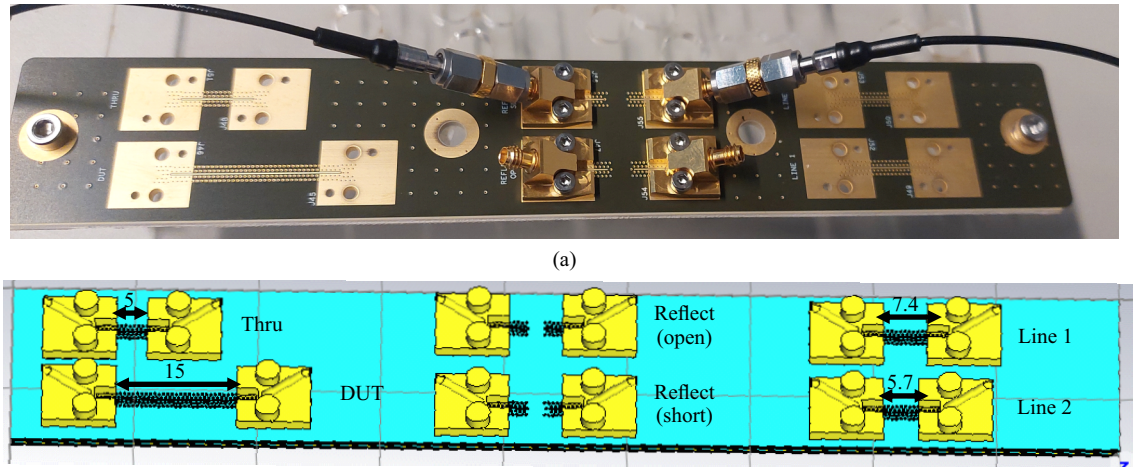

(a)

(b)

Figure 4. Illustration of the PCB test board for the 1-mm connectors: (a) prototype and (b) simulation model. Dimensions are in mm.

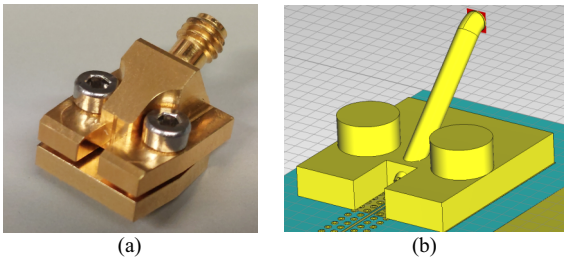

(a) (b)

Figure 5. 1-mm connector used in (a) measurements and (b) simulations.

of the divider are connected together with a resistance of $2Z_0$ (corresponding to 100 Ω in a 50-Ω environment) [16], [19]. At lower frequencies, this can easily be implemented using a lumped resistor, but it becomes more challenging when going towards higher millimetre-waves. The current power dividers use 100-Ω thin-film microwave resistors by Vishay in a 02016 size flip-chip type package that have been specified up to a frequency of 70 GHz [20]. At higher frequencies, reactive effects of the packaging start to affect the resistance value, which places a practical upper limit for the operating frequencies. To reach higher frequencies (e.g., above 100 GHz), the use of various integrated resistor techniques related to particular semiconductor fabrication processes may be required.

C. PCB With 1-mm Connectors

The second test structure consists of a coplanar waveguide (CPW) transmission line device under test (DUT) that has been implemented on a multi-layer PCB together with Thru-Reflect-Line (TRL) calibration structures. This structure is illustrated in Figure 4. The TRL kit can be used to de-embed the connector effects from the measurement results [21], [22]. For comparison, the kit includes a reflect standard implemented using both an open and shorted termination (either of which can be used). Additionally, the line standard has two versions of different lengths to make the calibration kit more broadband [23].

When moving higher up in frequency, accurate and reliable simulation models become increasingly important. In addition to providing estimates on the actual device performance, the models can be used in higher-order, system-level studies combining the operation of several individual components. For the purpose of this study, the modelling approach involves implementing a simulation model of the 1-mm connector used in the measurements. Figure 5 illustrates the actual connector and the 3D CAD model applied in simulations. The model, which has been created based on dimensions available in the data sheet, is a slightly simplified version of the real design, and it aims to capture the most essential features related to the 1-mm coaxial feed line and its connection to the transmission line on the PCB.

In the actual connector, the coaxial feed line is slanted. This poses a problem for the 3D simulation model in terms of positioning the feed port, since the simulation software requires all ports to align with the principal coordinate axes (x, y, or z axes). To solve this matter, a short extension/bend section has been implemented at the end of the coaxial cable to ensure a proper port alignment. This modification may have a slight impact on the connector performance, but the exact nature of the effect is difficult to quantify since it is not possible to simulate the original, slanted connector.

III. Characteristics of the Wilkinson Power Divider

The power divider has been designed for a 50-Ω impedance with the used substrate thickness, which is reflected in the width of the microstrip lines in the input and

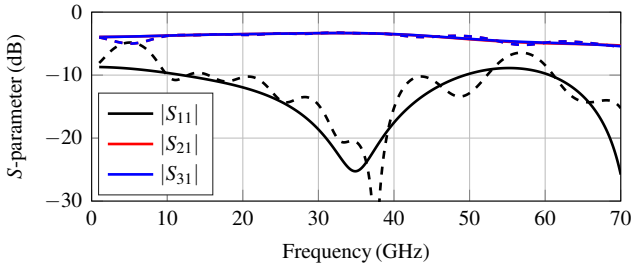

(a) Input side

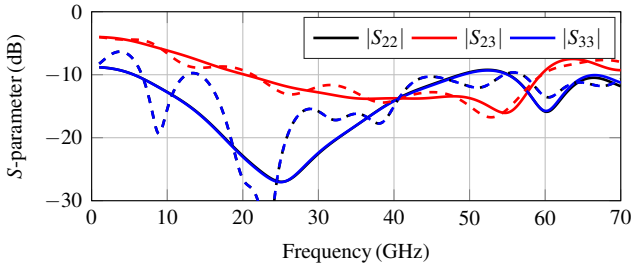

(b) Output side

Figure 6. Simulated S-parameters of the Wilkinson power divider. Solid lines: standalone component, dashed lines: with tapering to connector signal line width.

outputs (see Figure 3). However, this is different from the width of the SMPM connector signal pad, and for this reason a tapering section has been designed between the connector and divider to match the two impedance values. Figure 6 shows the simulated S-parameters of the power divider with and without the tapering. It can be seen that the effect of the tapering is not very significant for the overall operation.

In the measurements, the basic setup is that used with the 1-mm PCB. However, the SMPM connectors of the Wilkinson power divider require changes in the used cables. The modified setup is depicted in Figure 7. A cable with 1.85-mm connectors is mounted to the extender with a 1-mm-to-1.85-mm adapter, and a 1.85-mm-to-SMPM adapter is used to connect the 1.85-mm cable to an SMPM one. This configuration has been chosen based on available equipment. It should be noted that the highest frequency (70 GHz) in the simulations and measurements of the power divider is chosen based on the specifications of the resistor as well as the SMPM and 1.85-mm connectors rather than those of the 1-mm connector.

Simulated and measured S-parameters of the Wilkinson power divider are shown in Figure 8. The results generally agree well with each other, and the performance is good across a frequency range of about 10–50 GHz. The simulated and measured power divisions start to deviate from each other around 50 GHz, and this may be related to the dispersive effects of the resistor used.

Compared to simulations, the power division is not entirely equal between the output ports (as $|S_{21}| \neq |S_{31}|$).

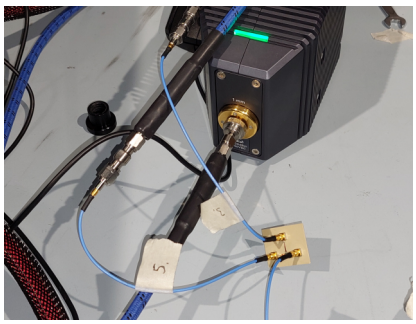

Figure 7. Photograph of the measurement setup used to characterise the Wilkinson power divider.

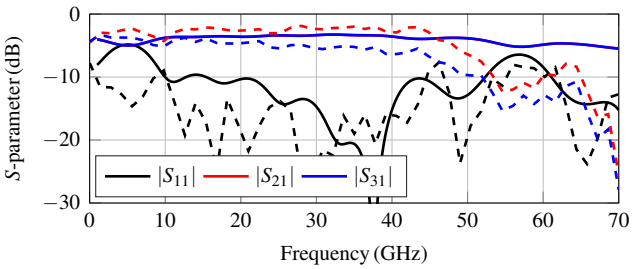

(a) Input side

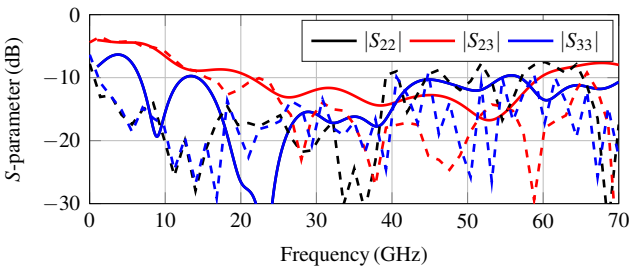

(b) Output side

Figure 8. Comparison of simulated (solid lines) and measured (dashed lines) S-parameters of the Wilkinson power divider.

According to simulations, this property should be equal as the structure is fully symmetrical. Reasons for this behaviour may be, e.g., inaccuracies in manufacturing and assembly, or effects coming from the measurement itself (such as bending of the cables and the non-ideal calibration technique used).

One drawback of the present connector and cable type is that there is no dedicated calibration structure for the particular assembly used. In order to approximate the cable effects, the insertion loss of the used cables has been measured, and this value has been subtracted from the measured $|S_{21}|/|S_{31}|/|S_{23}|$ results. The choice of calibration method was determined by the availability of suitable cables and adapters at the time of measurement.

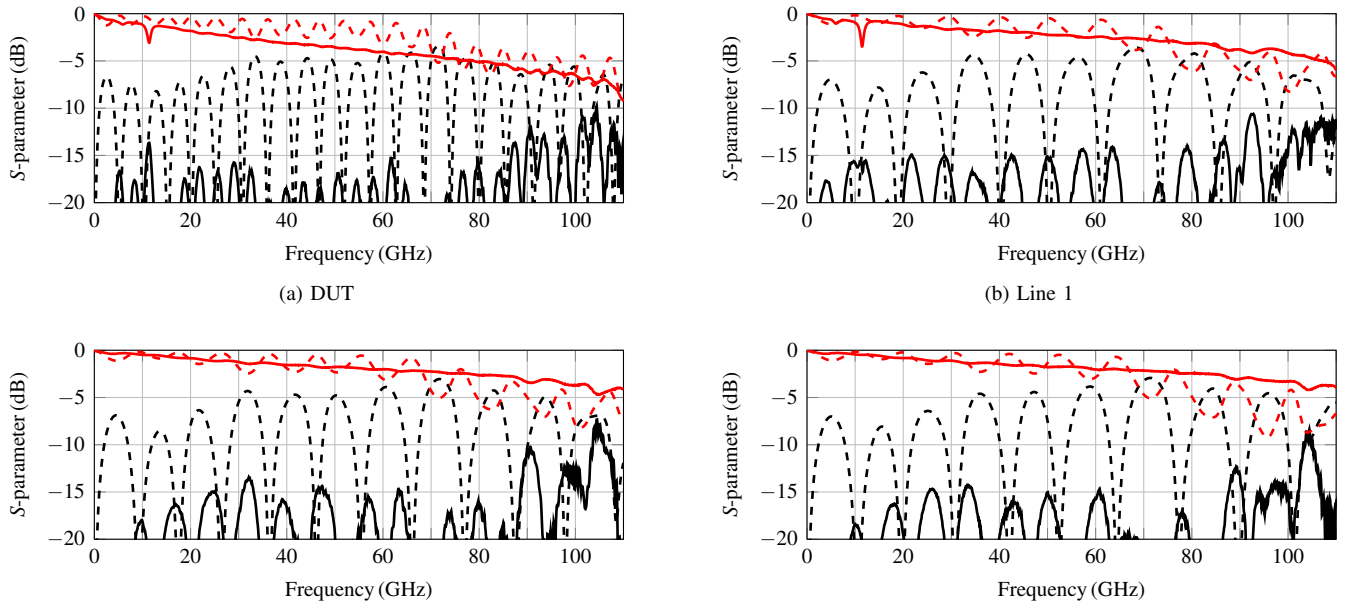

(a) DUT (b) Line 1

(c) Line 2 (d) Thru

Figure 9. Simulated and measured S-parameters of the DUT, line, and thru structures on the 1-mm connector PCB. The following colouring scheme is used in all figures: — = $|S_{11}|$ (meas.), - - = $|S_{11}|$ (sim.), — = $|S_{21}|$ (meas.), - - = $|S_{21}|$ (sim.).

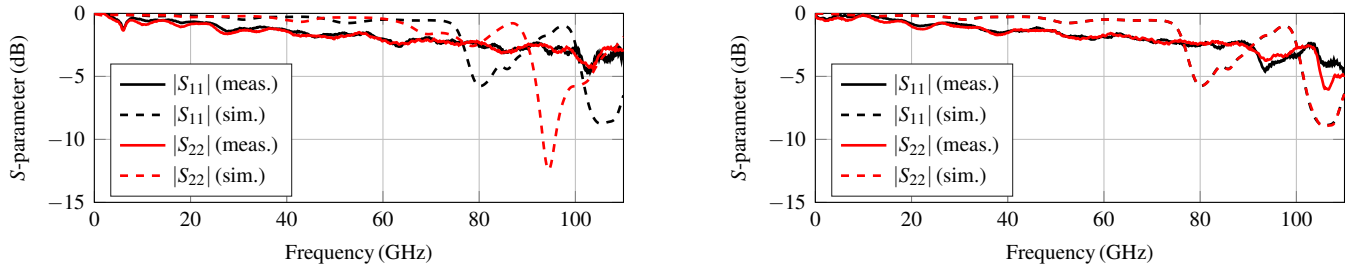

(a) Reflect (open) (b) Reflect (short)

Figure 10. Simulated and measured matching of the reflect open and short structures on the 1-mm connector PCB.

IV. Characteristics of the CPW Line Structures

The two-port S-parameters of the DUT and calibration standards have been characterised and the results are presented in Figures 9–11 (without taking into account any de-embedding). Measurements are shown as an average of two individual PCBs, both of which have been measured twice.

When looking at the simulated and measured results for the different lines and standards in Figure 9, it can be seen that they are generally following a similar trend across the frequency range. The matching level in the line structures (DUT, Line 1, and Line 2) is worse than in measurements. Taking into account the effect of the ripple in the simulated $|S_{21}|$ results, the insertion loss is comparable to the measured values. With the DUT and Line 1 structures, some of the measurements showed a noticeable dip in the $|S_{21}|$ curve around 11 GHz (the actual depth of the dip is slightly obscured by the averaging). Since this effect was not observed in simulations or all of the PCBs, it may be caused by some slight fabrication inaccuracies related to particular locations on specific boards.

In the two reflect structures, there are some small differences in the placement of the vias near the termination of the transmission line. Figure 10 shows the simulated and measured $|S_{11}|$ and $|S_{22}|$ parameters for the reflect open and short cases. Both ends of the short version are symmetric, but the open version has a small asymmetry. The effect of this asymmetry is more pronounced in simulations, with the probable cause being the via placement in the simulation model. Measured reflection coefficients in both ends of the reflect structure are in good agreement with both variants.

Figure 11 compares the simulated and measured isolation of the two reflect structures. Generally, both cases show

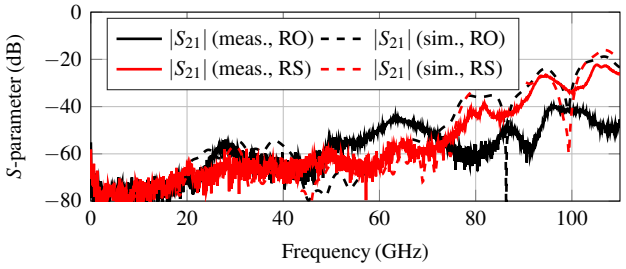

Figure 11. Simulated and measured isolation in the reflect open (RO) and short (RS) structures on the 1-mm connector PCB.

an isolation better than 20 dB (even better than 40 dB for the open version), and these levels are suitable for practical implementations of well-performing reflect standards.

The observed differences between simulated and measured results can be caused by slight inaccuracies between the material parameters used in simulations and those of the particular material used in the measurement, as well as by the 3D simulation model used for the connector. According to the substrate data sheet, the ε_r and $\tan\delta$ parameters have a quite stable frequency behaviour up to 50 GHz, but above that the precise characterisation of the dispersive effects would still require further studies. Additionally, the 1-mm connector model used in the simulations can have some inaccuracies and uncertainties especially related to the contact point between the coaxial centre pin and the transmission line. This results from a lack of certain dimensions or ambiguity thereof in the connector data sheet.

V. Conclusion

This work has investigated the design and implementation of RF test structures for higher millimetre-wave frequencies using a low-permittivity dielectric substrate. The material used to implement the measured structures has been utilised beyond the operation frequency characterised by the manufacturer. Of the test structures, the Wilkinson power divider shows good and broadband operation in both simulations and measurements, and the characteristics of the 1-mm connector structures show that the used dielectric material does not suffer too dramatic a reduction in performance when reaching frequencies around 100 GHz.

Results of this study can be used as a starting point for designing antennas, reconfigurable surfaces, high-speed digital interconnections, and even RF front ends with the current substrate material for above-100 GHz applications. Each of these components is an example of a structure with a very significant practical and commercial need when considering the continuous technological developments in the wireless industry. Future and on-going work includes utilising the present components in antenna and array designs, as well as characterisation of the material parameters of the substrate at higher millimetre-wave frequencies.

Acknowledgement

This work was supported by the Academy of Finland through the 6Genesis Flagship programme (grant no. 318927). The authors gratefully acknowledge Panasonic Corp. for providing the suitable material. Keysight Inc. has supported the research by donating measurement equipment.

The authors would like to thank Aspocomp for fabricating the 1-mm connector PCBs. Mr. Auno Latvalehto and Mr. Anssi Rimpiläinen are acknowlegded for manufacturing and soldering the Wilkinson power divider PCBs, respectively.

References

[1] J. G. Andrews *et al.*, "What will 5G be?" *IEEE J. Sel. Areas Commun.*, vol. 32, no. 6, pp. 1065–1082, June 2014.

[2] M. Latva-aho and K. Leppänen (eds.) "Key drivers and research challenges for 6G ubiquitous wireless intelligence," White Paper, 6G Flagship, University of Oulu, Finland, Sep. 2019.

[3] "5G evolution and 6G," White paper, NTT Docomo, Inc., Japan, Jan. 2020.

[4] A. Pärssinen *et al.* (eds.), "White paper on RF enabling 6G – opportunities and challenges from technology to spectrum," White paper, University of Oulu, Finland, 6G Research Visions, No. 13, Apr. 2021.

[5] N. Deferm and P. Reynaert, "A 120 GHz fully integrated 10 Gb/s short-range star-QAM wireless transmitter with on-chip bondwire antenna in 45 nm low power CMOS," *IEEE J. Solid-State Circuits*, vol. 49, no. 7, pp. 1606–1616, July 2014.

[6] J.-B. Doré *et al.*, "Technology roadmap for beyond 5G wireless connectivity in D-band," in *Proc. 2020 2nd 6G Wireless Summit (6G SUMMIT)*, Levi, Finland, Mar. 2020, 5 p.

[7] B. de Beelde *et al.*, "Material characterization and radio channel modeling at D-band frequencies," *IEEE Access*, vol. 9, pp. 153528–153539, 2021.

[8] T. Kakutani *et al.*, "Material design and high frequency characterization of novel ultra-low loss dielectric material for 5G and 6G applications," in *Proc. IEEE 2021 71st Electron. Compon. Technol. Conf. (ECTC)*, San Diego, CA, USA, 1 June - 4 July 2021, pp. 538–543.

[9] L. Cao, C.-F. Lo, H. Marchand, W. Johnson, and P. Fay, "Low-loss coplanar waveguides on GaN-on-Si substrates," *IEEE Microw. Wireless Compon. Lett.*, vol. 28, no. 10, pp. 861–863, Oct. 2018.

[10] T. Yu, K. Xue, K. Li, Y. Liang, and D. Yu, "Characteristics of 10-110GHz transmission lines on fused silica substrate for millimeter-wave modules," in *Proc. 2021 22nd Int. Conf. Electron. Packag. Technol. (ICEPT)*, Xiamen, China, Sep. 2021, 5 p.

[11] *IEEE Standard for Precision Coaxial Connectors (DC to 110 GHz),* IEEE Standard 287, 2007.

[12] Rosenberger Hochfrequenztechnik GmbH & Co. KG, Radio Frequency, Fiber Optic and High-Voltage Connectivity Solutions, Fridolfing, Germany, (accessed Feb. 16, 2022) [Online]. Available: https://www.rosenberger.com

[13] Panasonic low Dk / low Df material, Panasonic Corporation, Osaka, Japan, (accessed Feb. 14, 2022) [Online]. Available: https://industrial.panasonic.com/content/data/EM

[14] A. Lamminen *et al.*, "Characterization of interconnects on multilayer high frequency PCB for D-band," in *Proc. 2020 2nd 6G Wireless Summit (6G SUMMIT)*, Levi, Finland, Mar. 2020, 5 p.

[15] A. Lamminen, J. Säily, J. Ala-Laurinaho, J. de Cos, and V. Ermolov, "Patch antenna and antenna array on multilayer high-frequency PCB for D-band," *IEEE Open J. Antennas Propag.*, vol. 1, pp. 396–403, 2020.

[16] E. J. Wilkinson, "An *N*-way hybrid power divider," *IRE Trans. Microw. Theory Techn.*, vol. 8, no. 1, pp. 116–118, Jan. 1960.

[17] S. Horst, S. Bhattacharya, M. Tentzeris, and J. Papapolymerou, "Monolithic low cost Ka-band Wilkinson power dividers on flexible organic substrates," in *Proc. IEEE 2007 57th Electron. Compon. Technol. Conf. (ECTC)*, Sparks, NV, USA, 29 May - 1. June 2007, pp. 1851–1854.

[18] S. Horst, R. Bairavasubramanian, M. M. Tentzeris, and J. Papapolymerou, "Modified Wilkinson power dividers for millimeter-wave integrated circuits," *IEEE Trans. Microw. Theory Techn.*, vol. 55, no. 11, pp. 2439–2446, Nov. 2007.

[19] D. M. Pozar, *Microwave Engineering*, 3rd ed. New York: John Wiley & Sons, 2005.

[20] Vishay Intertechnology Inc., Electronic Components Manufacturer, Malvern, PA, USA, (accessed Feb. 16, 2022) [Online]. Available: https://www.vishay.com

[21] G. F. Engen and C. A. Hoer, "Thru-Reflect-Line: An improved technique for calibrating the dual six-port automatic network analyzer," *IEEE Trans. Microw. Theory Techn.*, vol. MTT-27, no. 12, pp. 987–993, Dec. 1979.

[22] R. B. Marks, "A multiline method of network analyzer calibration," *IEEE Trans. Microw. Theory Techn.*, vol. 39, no. 7, pp. 1205–1215, July 1991.

[23] V. Teppati, A. Ferrero, and M. Sayed (eds.) *Modern RF and Microwave Measurement Techniques*, Cambridge University Press, 2013.